Chemical Engineering Journal 150 (2009) 492–501

Contents lists available at ScienceDirect

Chemical Engineering Journal

journal homepage: www.elsevier.com/locate/cej

Evaluation of the mixing performance of three passive micromixers

Shakhawat Hossain, M.A. Ansari, Kwang-Yong Kim*

Department of Mechanical Engineering, Inha University, 253 Yonghyun-Dong Nam-Gu, Incheon, 402-751, Republic of Korea

ARTICLE INFO

Article history:
Received 25 December 2008
Received in revised form 15 February 2009
Accepted 25 February 2009

Keywords:
Micromixer
Diffusion
Laminar flow
Numerical analysis
Mixing index

ABSTRACT

This work presents a numerical investigation on mixing and flow structures in microchannels with different geometries: zig-zag; square-wave; and curved. To conduct the investigation, geometric parameters, such as the cross-section of the channel, channel height, axial length of the channel, and number of pitches, are kept constant for all three cases. Analyses of mixing and flow fields have been carried out for a wide range – 0.267–267 – of the Reynolds number. Mixing in the channels has been analyzed by using Navier–Stokes equations with two working fluids, water and ethanol. The results show that the square-wave microchannel yields the best mixing performance, and the curved and the zig-zag microchannels show nearly the same performance for most Reynolds number. For all three cases, the pressure drop has been calculated for channels with equal streamwise lengths. The curved channel exhibits the smallest pressure drop among the microchannels, while the pressure drops in the square-wave and zig-zag channels are approximately the same.

1. Introduction

The potential applications of microfluidic systems are diverse and widespread. The systems have helped to modernize various fields of science, in particular, the biomedical and biochemical sciences, due to their application in areas such as DNA analysis, cell storage [1], high-throughput screening, dynamic cell separators [2], etc. Mixing in microchannels plays an important role in Bio Micro-Electro-Mechanical Systems (BioMEMS) and micro-total analysis systems.

At very low Reynolds numbers, mixing takes relatively long time since viscous effects due to molecular diffusion dominate the mixing process. To enhance the mixing in microchannels, one effective method is to stretch and fold fluids to generate chaotic advection and to increase the interfacial area between different fluids.

Micromixers that are reported in the literature can be classified into two categories: active and passive micromixers. Active micromixers use additional structures or external sources including ultrasonic vibration, dielectrophoresis, electrohydrodynamic, electroosmosis, and magnetic force, to stir the fluids. Passive micromixers do not require external energy; the mixing process relies entirely on diffusion or chaotic advection. Passive mixers can be further classified into several categories: lamination micromixer, injection micromixer, etc. In lamination mixers, the fluid streams are split into several small streams, which are later joined in a mixing channel [3]. In contrast to lamination mixers, an injection mixer splits only one stream into many substreams in the form of microplumes, which increase the contact surface and decrease the mixing path. In addition, active micromixers are generally more complex and can thus be difficult to operate, fabricate, clean, and integrate into microfluidic systems. Passive mixers are used in most microfluidic applications.

In a passive micromixer, mixing can be improved by modifying the geometry. Ansari and Kim [4] optimized the design of a staggered herringbone grove micromixer by using surrogate modeling. The main concept in this design is to increase the interfacial area between two fluids by creating a transverse flow. Chen and Cho [5] analyzed mixing characteristics for an electrokinetically driven flow through microchannels with a wavy surface. The wavy shape increases the mixing performance by increasing the interfacial contact area between two fluid streams in comparison with a simple, straight microchannel. In some microfluidic applications, a recirculation-flow technique is used to increase the mixing interface.

Liu et al. [6] studied both numerically and experimentally the mixing in a three-dimensional serpentine microchannel, a square-wave microchannel, and a straight microchannel. In the flow-visualization experiments, they found that for Reynolds numbers from 6 to 70, the three-dimensional serpentine channel shows a significantly better rate of mixing than the square-wave and straight channels. They also reported that at a Reynolds number of 70, the mixing capability of the three-dimensional serpentine channel is 1.6 times more than that of the square-wave channel and 16 times more than that of the straight channel. Ansari and Kim [7] performed a parametric study on the performance of a three-dimensional serpentine channel with repetitive, L-shaped units. They investigated the effect of geometric parameters on mixing and fluid flow, and reported that the bends in the serpentine

* Corresponding author. Tel.: +82 32 872 3096; fax: +82 32 868 1716.
E-mail address: kykim@inha.ac.kr (K.-Y. Kim).

1385-8947/$ – see front matter © 2009 Elsevier B.V. All rights reserved.
doi:10.1016/j.cej.2009.02.033

Nomenclature

D_h	hydraulic diameters
c	mass fraction
H	channel height (mm)
Lc	length of the main channel (mm)
Lo	length of the channel inlet (mm)
Le	length of the channel outlet (mm)
W	channel width (mm)
Pi	pitch length (mm)
N	number of sampling points
Re	Reynolds number
M	mixing index

Greek letters

μ	absolute viscosity of fluid ($kg\,m^{-1}\,s^{-1}$)
ρ	fluid density ($kg\,m^{-3}$)
σ	variance
α	scalar diffusivity
θ	angle of turn in the zig-zag channel

channel strongly affect the flow structure and hence, mixing. The study shows that mixing is significantly dependent upon geometric parameters. Chen and Yang [8] performed both numerical and experimental investigations on mixing in zigzag microchannel with electroosmotic flow, and reported that due to the racetrack effect diffusion within the fluids increases and hence the mixing performance is enhanced.

Mengeaud et al. [9] conducted experimental and numerical investigations of mixing in zig-zag microchannels. Their results indicate that at a certain value of the Reynolds number, recirculation zones form around the turns of the microchannel, which increases the mixing index. They reported that the critical Reynolds number is approximately 10, indicating that transition in the mixing performance occurs at a comparatively low Reynolds number. As the Reynolds number increases, vortices form at the turns of the microchannel. These vortices flow through a narrow region; thus, the diffusion length is reduced and the mixing performance is improved.

Vanka et al. [10] undertook a numerical study of scalar mixing in curved channels at low Reynolds numbers and reported that at low Reynolds numbers, mixing in a curved channel is not very effective because of the low intensity of secondary flow. With an increase in the Reynolds number, the level of secondary flow increases, and this becomes another way of enhancing mixing. Due to the centrifugal force, secondary flows are induced, and the fluid in the middle of the channel is pushed to the outer sides of the turns.

For various Reynolds and Schmidt numbers, Khmar et al. [11] analyzed the mixing performance in a curved microchannel with a circular cross-section and varying curvature ratios. At higher Schmidt numbers, the mixing of fluids considerably improves at Re ~10 but is not effective at Re ~0.1. This is also described in the study of Vanka et al. [10].

Sudarsan and Ugaz [12] analyzed mixing in a compact, spiral-shaped microchannel at Reynolds numbers ranging from 0.02 to 18.6 and reported that at low Reynolds numbers, mixing is mainly governed by diffusion, and at higher Reynolds numbers, secondary flows are induced that enhance mixing. Chang and Cho [13] analyzed mixing with four different types of static micromixers; they used micro-blocks that induce swirl flows. Their designs create a rotational flow field that can mix the flow for a wide range of flow rates.

Park et al. [14] designed a passive micromixer that induces fluid rotation for mixing the fluids at low and high Reynolds numbers. They reported that due to the stretching and folding of the interface between fluids, the rotation of fluids increases and enhances mixing. Jeon et al. [15] proposed a passive micromixer with a side-channel for creating recycle flow at Reynolds numbers of 7, 14, and 28. They applied computational fluid dynamics to design and optimize the geometry for creating recycle flow. The flow circulation increases the mixing efficiency.

As mentioned above, a variety of experimental and numerical studies have been carried out for different types of passive micromixers. However, not many of the reported investigations compare the flow and mixing mechanisms of different geometries. The present study conducts a computational fluid dynamic investigation of mixing performance for three different microchannels, i.e., a zig-zag, square-wave, and curved channels. Two miscible fluids, water and ethanol, are used for mixing.

2. Numerical formulation

Schematic diagrams of the curved, square-wave, and zig-zag channels are shown in Fig. 1. The height of the channel (H), the axial length of main channel (Lc), the width of the channel cross-section

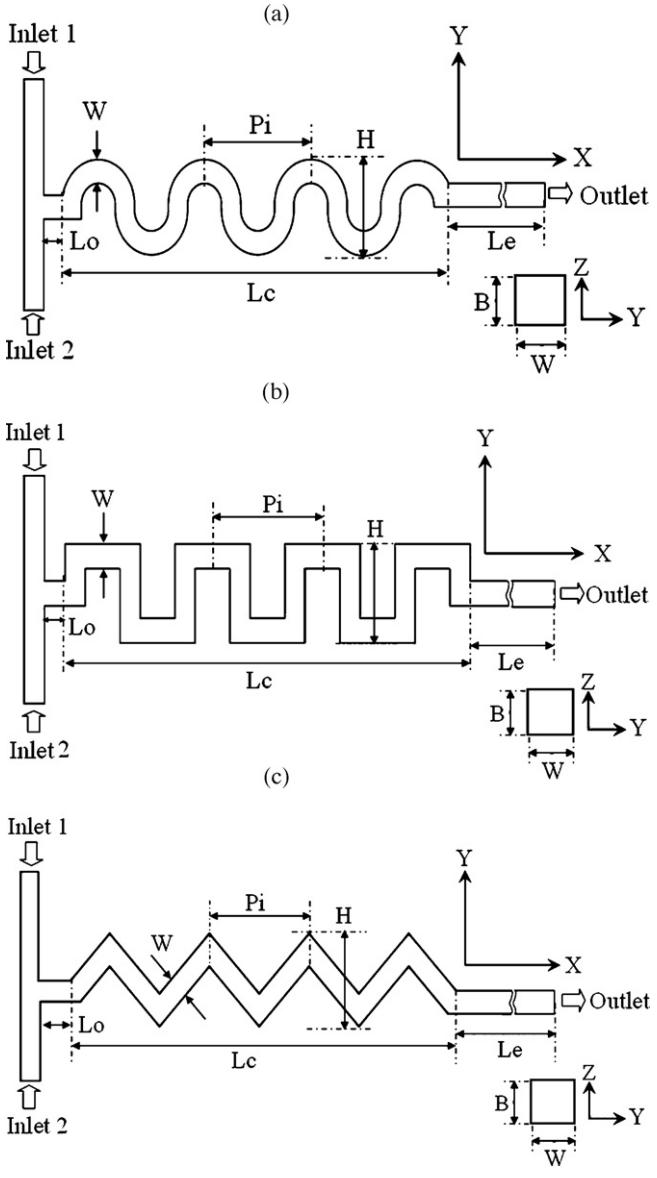

Fig. 1. Schematic diagrams: (a) curve channel; (b) square-wave channel; and (c) zig-zag channel.

Table 1
Properties of fluids at 20 °C.

Fluid	Density (kg m^{-3})	Viscosity (kg m^{-1} s^{-1})	Diffusivity (m^2 s^{-1})
Water	9.998×10^2	0.9×10^{-3}	1.2×10^{-9}
Ethanol	7.890×10^2	1.2×10^{-3}	1.2×10^{-9}

(W), the length of the channel cross-section in z direction (B), and the number of repeating units are kept constant for all three geometries. The dimensions are as follows: $H = 0.4$ mm; Lc = 2.0 mm; $W = 0.1$ mm; $B = 0.1$ mm; Pi = 0.56 mm; Lo = 0.1 mm; and Le = 1.8 mm. Thus, the aspect ratio of the channel cross-section, W/B is unity. The number of repeating units is four. In the zig-zag channel, the corner angle (θ) is 90°, and in the curved channel, the radii of the inner and outer circles are 0.0878 mm and 0.1878 mm, respectively. The cross-sectional size of the inlet channels is same as that of the main channel, i.e., 0.1 mm × 0.1 mm. The two inlets, Inlet 1 and Inlet 2, are merged in the main microchannel with a T-joint, as shown in Fig. 1. Water and ethanol are used as the two operating fluids for mixing. The properties of the water and ethanol have been taken at 20 °C and are listed in Table 1. The diffusivity for both water and ethanol is 1.2×10^{-9} m^2 s^{-1}.

To analyze the flow and mixing in the micromixers, the commercial CFD-code, ANSYS CFX-11 [16], has been used. By using the finite-volume method, the ANSYS CFX-11.0 code solves the Navier–Stokes equations. The solver solves the steady continuity and momentum (Navier–Stokes) equations. ANSYS CFX is capable of modeling fluid mixtures that comprise many separate physical components, where each component may have a distinct set of physical properties. For calculating the fluid flow, the ANSYS CFX-Solver will calculate the appropriate average values of the properties for each control volume in the flow domain. These average values depend on the values of the component properties and the percentage of each component that is present in the control volume. In the case of multi-component fluids, the assumption is made that the fluids are mixed at the molecular level and that the properties of the fluids are dependent on the proportions of the components. It is also assumed that the mass fraction arises through convection and diffusion. The differential motions of the individual components in the mixture are computed by the relative mass flux terms. This term is modeled by the effect of concentration gradients, pressure gradients, etc.

ANSYS ICEM 11.0 is used to make hexahedral grids for the full model. To obtain accurate simulations of the mixing, it is necessary to examine and modify the quality of the mesh. To analyze the actual mixing phenomena in the microchannels, Navier–Stokes equations in combination with an advection–diffusion model are applied. The numerical simulation is not free from numerical diffusion errors, which arise from the discretization of the convection terms in the Navier–Stokes equation. Numerical diffusion cannot be completely ignored; however, it can be minimized by adopting certain techniques [17].

The velocity at the inlets and zero static pressure at the outlet are specified as the boundary conditions. Pure ethanol is assigned to Inlet 1, and pure water to Inlet 2. The no-slip condition was applied at the walls. The solutions are considered to have attained convergence when the value of the root-mean-squared (rms) relative residual is at most 10^{-6}.

The mixing efficiency is quantified by calculating the variance of the mixture in the micromixer. To evaluate the degree of mixing in the micromixer, the variance of the mass fraction of the mixture in a cross-section that is normal to the flow direction is defined as follows:

$$\sigma = \sqrt{\frac{1}{N}\sum (c_i - \bar{c}_m)^2}$$

In the above definition, N is the number of sampling points inside the cross-section, c_i is the mass fraction at sampling point, i, and c_m is the optimal mixing mass fraction. In this work, N on each plane

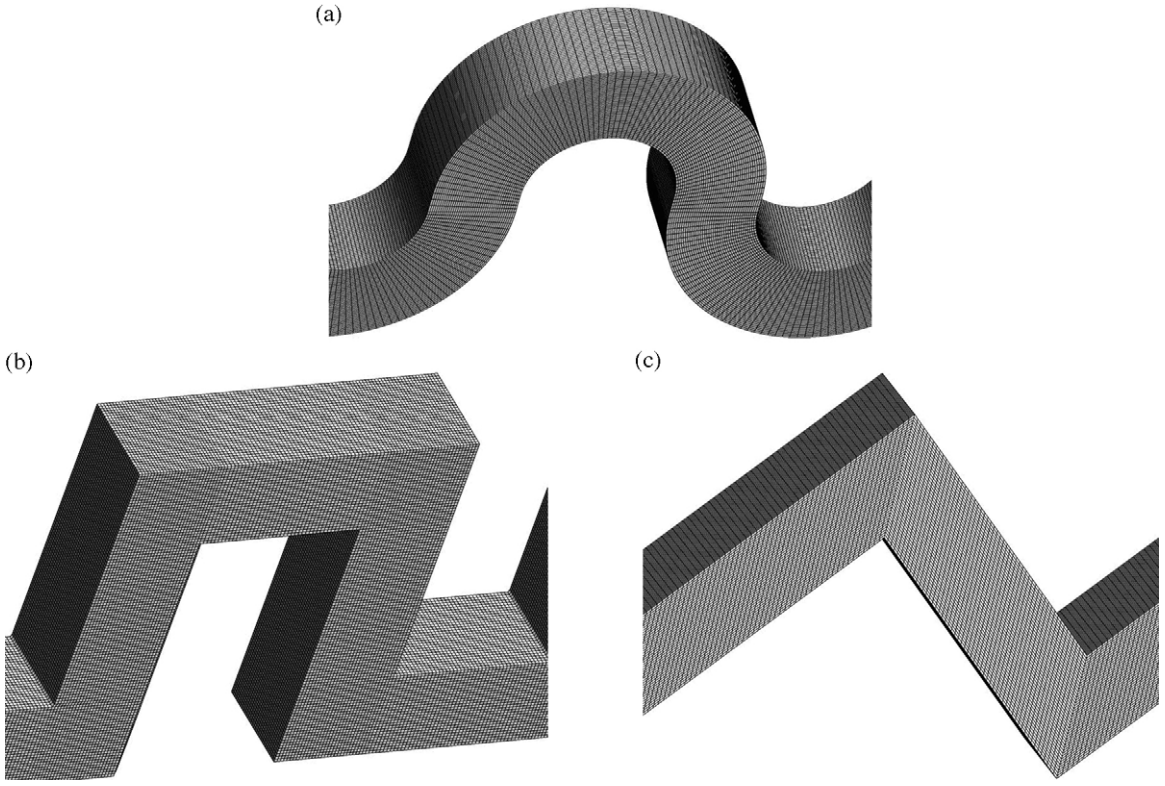

Fig. 2. Hexahedral grid systems: (a) curve channel; (b) square-wave channel; and (c) zig-zag channel.

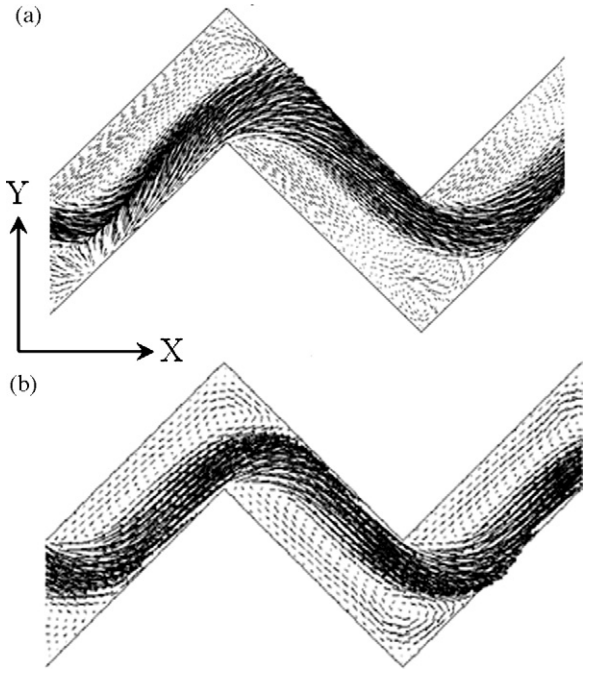

Fig. 3. Comparison of the present results with reference results at Re = 267: (a) vector plot for the present numerical simulation and (b) reference results [9].

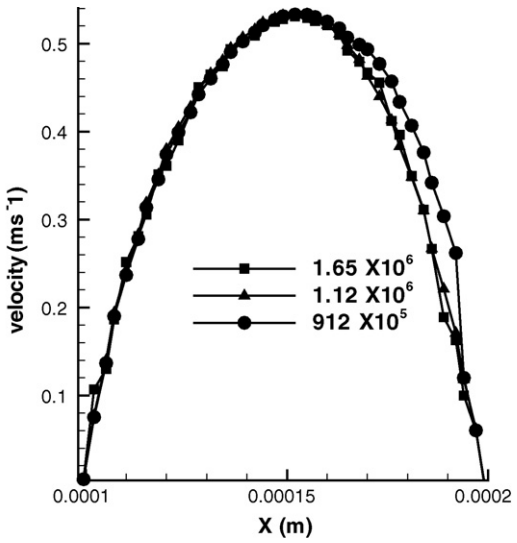

Fig. 4. Local velocity profiles for zig-zag channel with various numbers of grids.

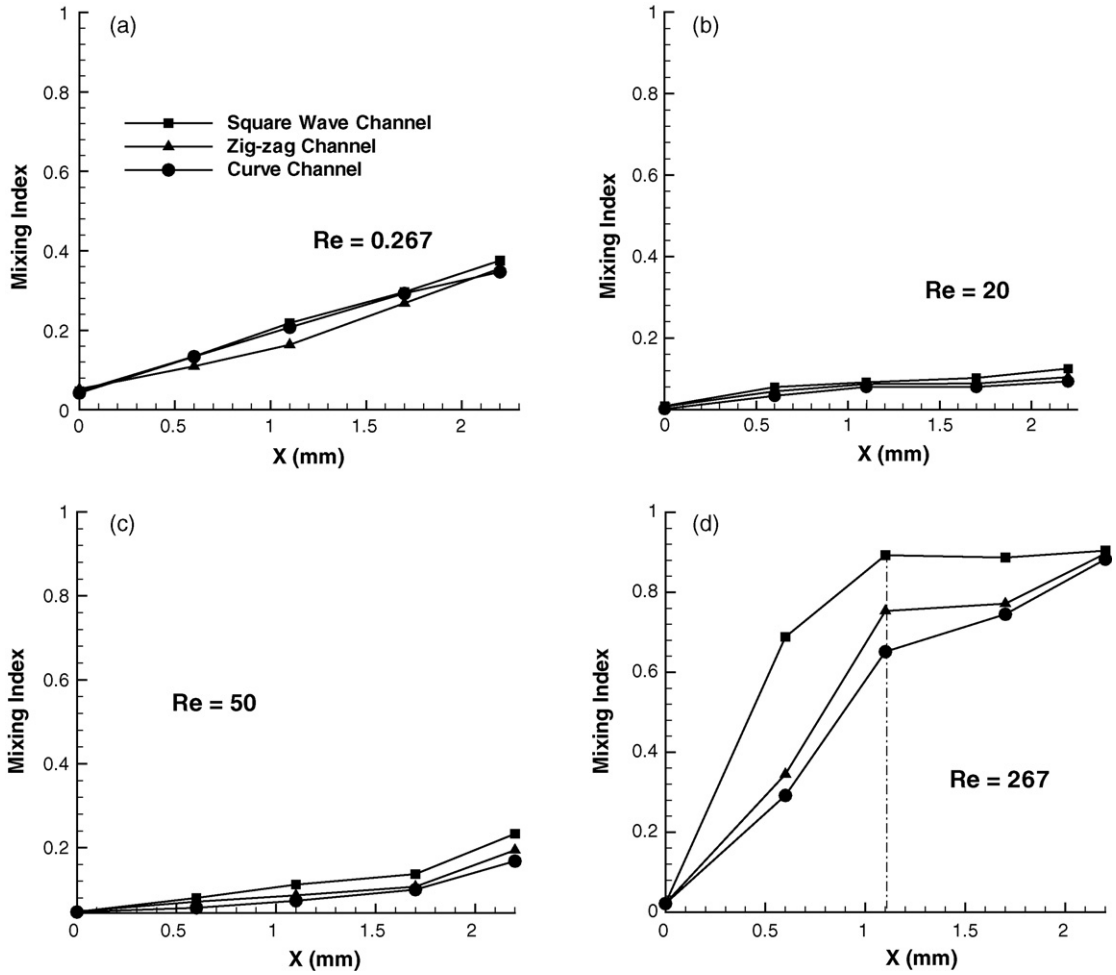

Fig. 5. Distributions of the mixing index with fixed axial length: (a) Re = 0.267; (b) Re = 20; (c) Re = 50; and (d) Re = 267.

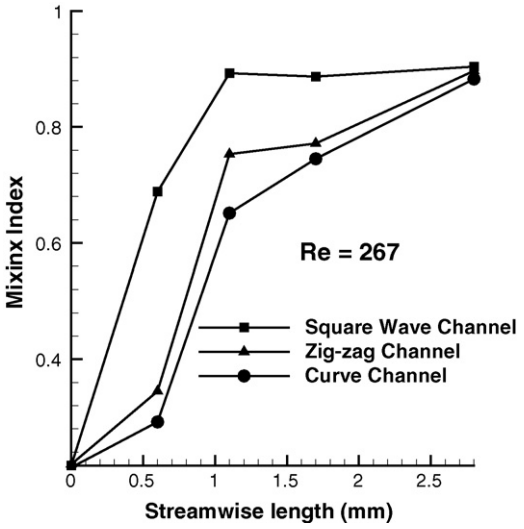

Fig. 6. Distributions of mixing index with fixed streamwise length at Re = 267.

was more than 550 in order to ensure high accuracy, and the sampling points are equidistant on the cross-sectional plane. The values at the sampling points are obtained by interpolations with the values at adjacent computational grids. To quantitatively analyze the mixing performance of the micromixer, the mixing index is defined as follows:

$$M = 1 - \sqrt{\frac{\sigma^2}{\sigma_{\max}^2}}$$

where, σ is the standard deviation of the concentration across the channel in a cross-section at any specific longitudinal location, and $\sigma_{\max}$ is the maximum standard deviation at the inlet of the main channel. A greater mixing index indicates a higher mixing quality: the value of this mixing index is thus 0 for completely separate streams (for which $\sigma = \sigma_{\max}$), and 1 for completely mixed streams (for which $\sigma = 0$). For all geometries, the mixing index has been calculated at every turn for comparing the results across geometries.

3. Results and discussion

To find out the optimal number of grids, it is necessary to verify that the solution is grid-independent. Five different structured grid systems, wherein the number of grids ranged from 2.01×10^5 to 1.65×10^6, were tested for each microchannel. Finally, from the results of the grid-dependency test, 1.12×10^6 was selected

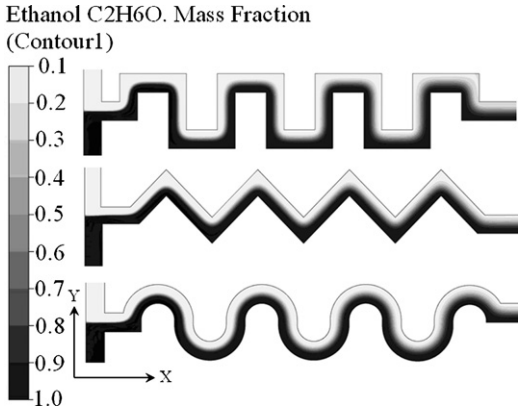

Fig. 7. Distributions of the concentration of ethanol for three geometries on the *xy*-plane at the middle of the channel cross-section height (Re = 0.267).

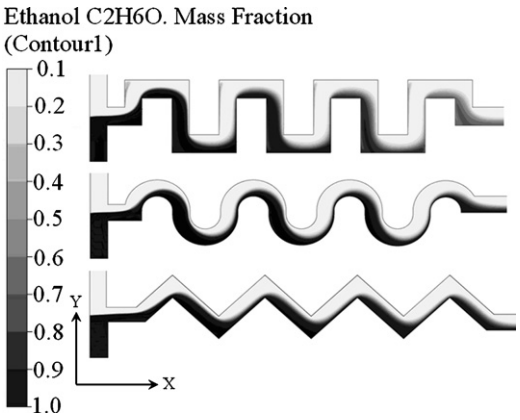

Fig. 8. Distributions of the concentration of ethanol for three geometries on the *xy*-plane at the middle of the channel cross-section height (Re = 50).

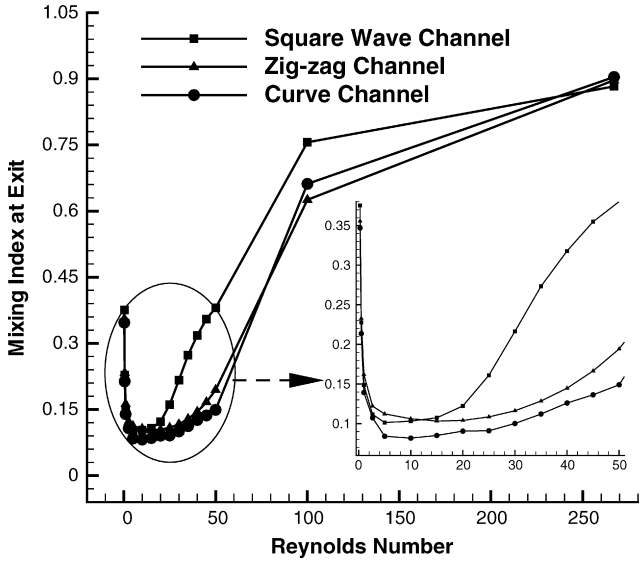

Fig. 9. Variations of the mixing index with the Reynolds number at the exit with fixed axial length.

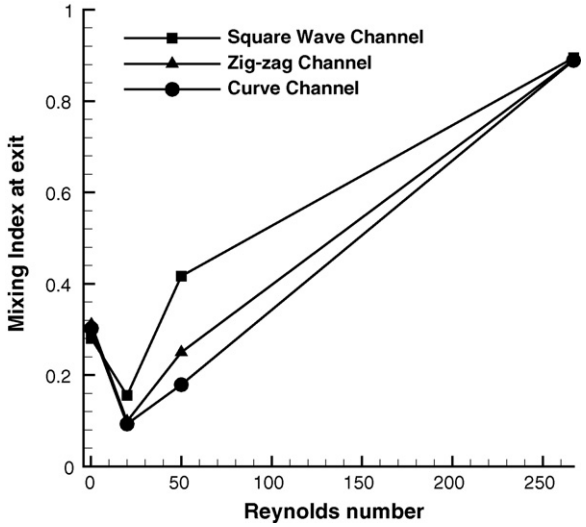

Fig. 10. Variations of the mixing index with the Reynolds number at the exit with fixed streamwise length.

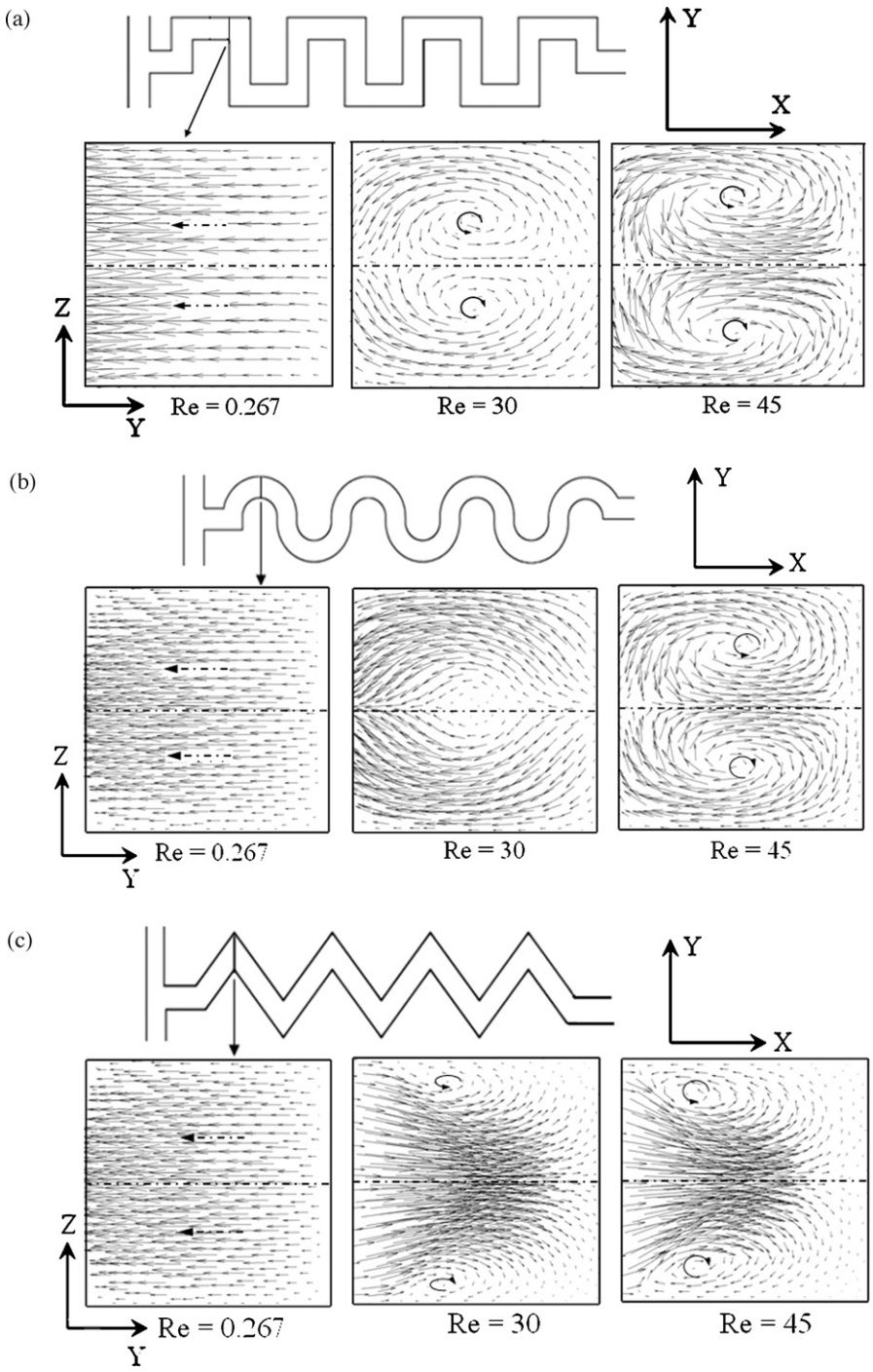

Fig. 11. Velocity–vector plots for the three different channels on the *yz*-plane: (a) square-wave channel; (b) curved channel; and (c) zig-zag channel.

as the optimal number of grids. Examples of the structured grid system employed in this work are shown in Fig. 2. And, the size of the cell in the main channel has been varied from $3.31 \times 10^{-3} \times 3.66 \times 10^{-3}$ mm^2 to $3.38 \times 10^{-3} \times 3.72 \times 10^{-3}$ mm^2.

The present results are compared with the numerical results of Mengeaud et al. [9] for the same channel width and Reynolds number shown in Fig. 3. The velocity vectors have been plotted on the *xy*-plane at the middle of the height of the channel cross-section. The velocity vectors are almost the same as those yielded by prior numerical results [9]. Fig. 4 shows the local velocity profiles for different grid numbers at the corner of the zig-zag channel. And, the figure represents that 1.12×10^{-6} is the number of grids that gives grid-independent solution.

Fig. 5 shows the distributions of the mixing index for three channels at different Reynolds numbers, viz., 0.267, 20, 50, and 267, respectively. At low Reynolds numbers, the mixing is limited by molecular diffusion and the mechanical stirring is ineffective at $\mathrm{Re} \ll 1$ [18]. At a Reynolds number of 0.267, the mixing index increases almost linearly along the channel. At the exit of the square-wave channel, the three channels show nearly same mixing index. The mixing at low Reynolds numbers is dominated by the residence time and depends on the total path of the flow. At a Reynolds number of 20, the mixing capability of the square-wave channel is 1.34 times larger than that of the zig-zag and curved channels. Different mixing behaviors are depicted at various Reynolds numbers. A comparison of the mixing index between Reynolds numbers of 50

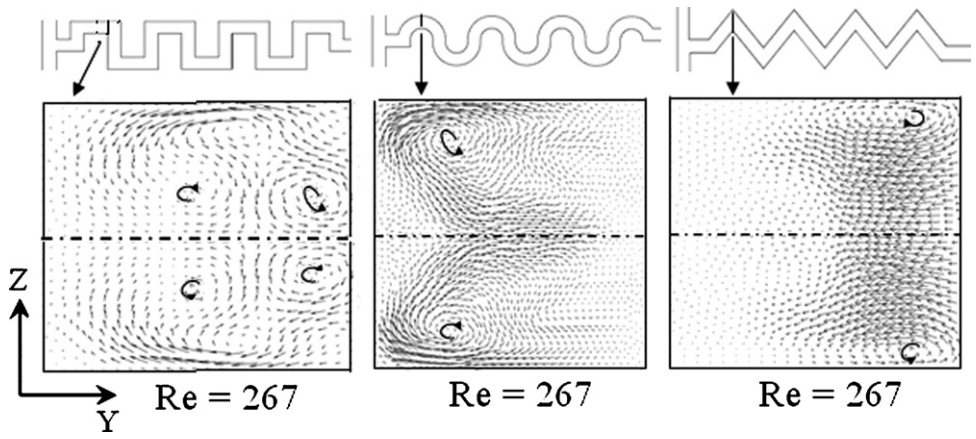

Fig. 12. Velocity–vector plots for the three different channels on the *yz*-plane at a Reynolds number of 267: (a) square-wave channel; (b) curved channel; and (c) zig-zag channel.

and 267 reveals contrary behaviors of the mixing-index gradient. The gradient of the mixing index almost monotonically increases in the *x*-direction at Re = 50 but decreases at Re = 267. At Re = 267, the mixing indexes at the ends of the micromixers are almost the same for all the three shapes of the microchannel, unlike the case of other Reynolds numbers. The mixing index reaches its maximum value at the middle of the channel in the case of the square-wave channel. Due to the stronger secondary flows in the microchannel, a high mixing performance is evinced by the square-wave channel at most Reynolds numbers. Fig. 6 shows the distributions of the mixing index with a fixed streamwise length at Reynolds number, 267. The streamwise length is fixed as 2.8 mm. The distributions are quite similar to the case with fixed axial length shown in Fig. 5(d).

The distributions of the concentration of ethanol for the three channels at a Reynolds number of 0.267 are shown in Fig. 7. The figure shows that at this low Reynolds number, the mixing increases steadily along the length of the channel, as shown in Fig. 5(a). The paths of two fluid flows are nearly parallel to each other, and there is no secondary flow. In the square-wave channel, due to the longer path of the flow, the residence time becomes longer and the mixing efficiency also becomes higher. The distributions of the concentration at a Reynolds number of 50 are shown in Fig. 8. In comparison with the distributions for Re = 0.267 (Fig. 7), owing to a high Reynolds number, which encourages an adverse pressure gradient and vortical flow, the vortical flow occupies a large region and the agitation of circulation is increased. During turning of the flow, flow near the inner corner accelerates, and flow near the outer corner decelerates. The degree of acceleration is controlled by the degree of turning [19]. The degree of the acceleration determines the characteristics of the induced vortex. Due to the centrifugal force, the interface between fluids is closer to the inner wall before turning and nearer to the outer wall after turning.

Fig. 9 shows the distributions of the mixing index at the exits of different channels at various Reynolds numbers, namely, 0.267, 0.5, 1, 2.67, 5, 10, 15, 20, 25, 30, 35, 40, 45, 50, 100, and 267. As the Reynolds number increases, the level of the mixing index increases for all three microchannels, except in the range of low Reynolds numbers. At low Reynolds numbers (i.e., smaller than 5–15, depending on the type of the microchannel), transverse flow is negligible, and thus, mixing occurs due to only the diffusion of fluid molecules, as a result of the higher residence time and lower overall velocity. Therefore, the mixing is enhanced rapidly as the Reynolds number decreases in this range. At these lower Reynolds numbers, the square-wave channel shows relatively higher mixing performance than the other microchannels due to the longer residence time that arises from the longer path of flow, as shown in Fig. 7. In the case of the square-wave and curved channels, the mixing index is minimized at a Reynolds number of 5, while for the zig-zag microchannel, the mixing index is minimized at a Reynolds number of 15. In the range of 5–15 for the Reynolds number, the mixing index varies only slightly in all the three cases. In this range, the residence time is insufficient but the transverse flow is still inactive; thus, the mixing index realizes the minimum values. However, beyond this range of the Reynolds number, the residence time decreases as the Reynolds number increases, while the transverse flow rapidly becomes active. It is noted that the square-wave channel shows a rapid increase in the mixing index immediately beyond a Reynolds number of 15, while the other channels show a region of gradual increase prior to the rapid increase that commences near a Reynolds number of 50. The bend in the microchannel induces stirring and also enhances the mixing performance [9]. The strength of the secondary flow in the curved channel increases more rapidly, when compared to the zig-zag channel, in the range of 50–100 for the Reynolds number. Thus, at a Reynolds number of 100, the curved channel overtakes the zig-zag channel in terms of the mixing performance. Since the square-wave microchannel has a larger number of bends than the zig-zag microchannel, the square-wave microchannel provides greater mixing than the zig-zag microchannel. However, at a Reynolds number of 267, the mixing index at the exit approaches the limiting value of about 0.9 in all the three cases. In the range of high Reynolds numbers, i.e., from 15 to 250, where the transverse motion of the flow prevails in the mixing process, the square-wave microchannel shows the best mixing performance, and the curved and the zig-zag microchannels show nearly the same performance as one another.

Fig. 10 compares the mixing indexes at the channel exit with fixed streamwise length of different channels at various Reynolds numbers, namely, 0.267, 20, 50, and 267. The fixed streamwise length has been taken as 2.8 mm. In case of the curved and the square-wave channels, this streamwise length (2.8 mm) covers 92% and 70% of the axial length fixed for Fig. 1(a) and (b), respectively, while for the zig-zag channel it covers the entire axial length. At low Reynolds number 0.267, mixing is diffusive and depends on mixing path of fluids. Due to the fixed streamwise length, at this low Reynolds number every channel shows same performance. At Reynolds numbers, 20 and 50, mixing index in square-wave channel shows the highest mixing performance as in Fig. 9. Due to the strong secondary flows, every channel shows same mixing performance at Reynolds number, 267, while the previous figure (Fig. 9) for the fixed axial length shows slightly different values of the mixing index. This indicates that the mixing index is determined by the streamwise length of the channel regardless of the channel type at this Reynolds number.

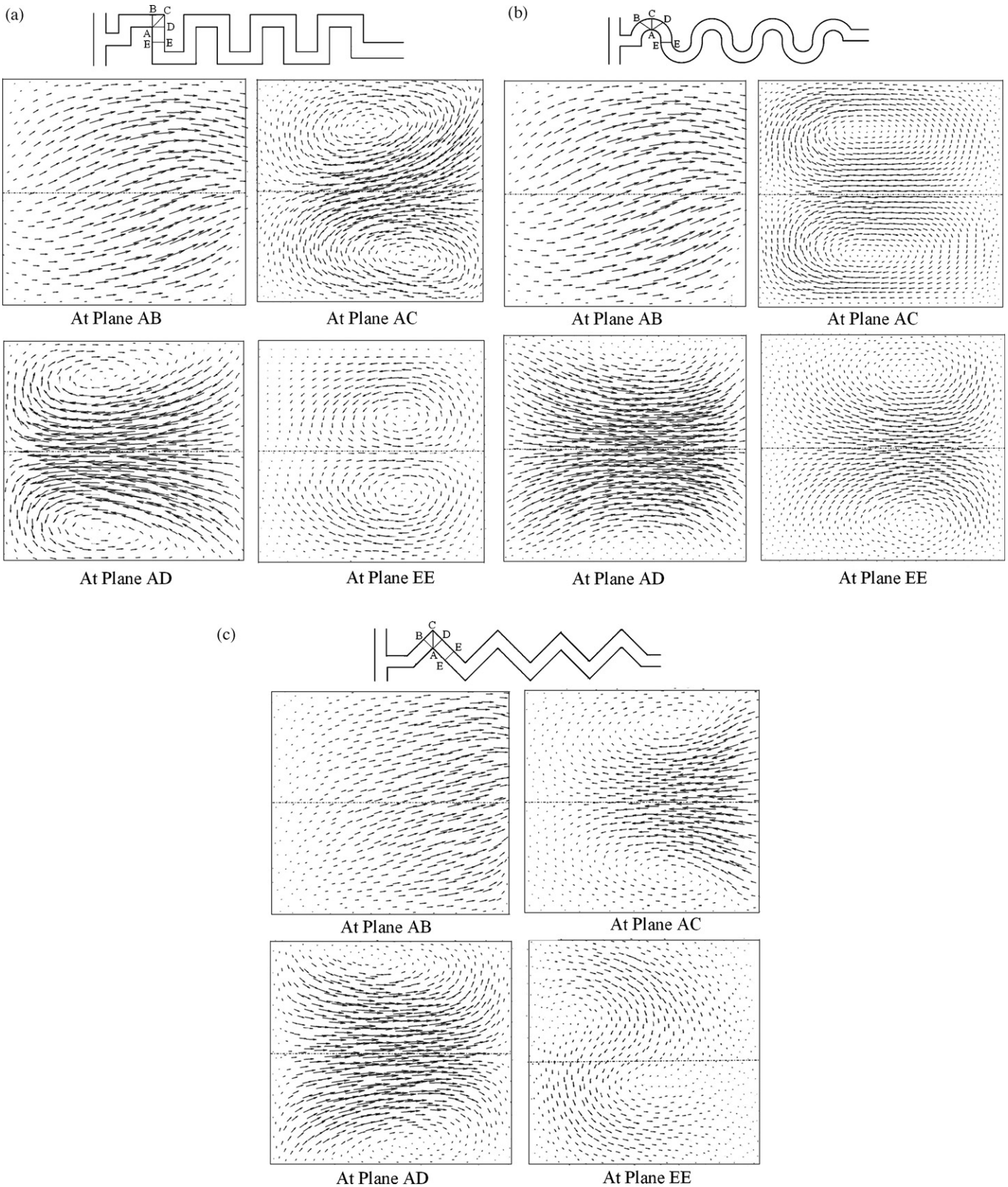

Fig. 13. Velocity–vector plots for the three different channels at different positions at a Reynolds number of 50: (a) square-wave channel; (b) curved channel; and (c) zig-zag channel.

Fig. 11 shows the vector plots on the *yz*-plane for the three different channels at Reynolds numbers of 0.267, 30, and 45. At a Reynolds number of 0.267, the flow pattern is almost the same in every channel, and the velocity vectors are parallel to the channel wall everywhere in the cross-section. Transverse vorticals flows are generated as the Reynolds number increases. At a Reynolds number of 30, in the square-wave and zig-zag channels where the cross-section that is of interest is located at a turn, two small vortices are

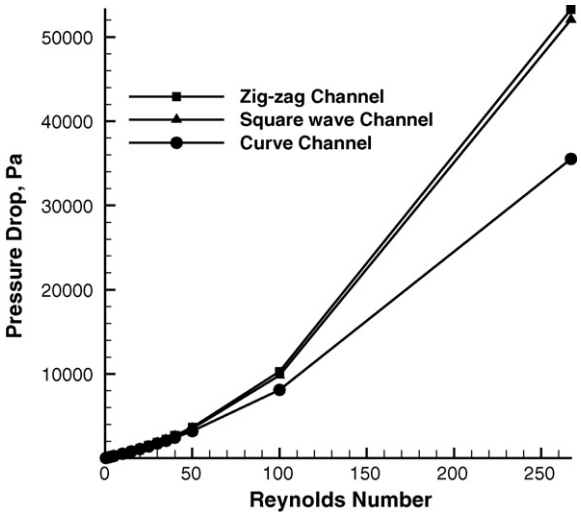

Fig. 14. Variation of the pressure drop with the Reynolds number for the three geometries.

generated in the channels. However, the vortical motion is much stronger in the square-wave channel, and thus, at this Reynolds number, viz., 30, the square-wave channel shows by far the highest mixing performance and the zig-zag channel follows next, as shown in Fig. 9. At a Reynolds number of 45, the formation of two symmetric, counter-rotating vortices is commonly found in all channels.

Fig. 12 shows the velocity–vector plots on the *yz*-plane in a square-wave channel, curved channel, and zig-zag channel at Re = 267. The flow is visualized with the presence of strong transverse flow structures in all the three channels. In the case of the curved and zig-zag channels, this figure shows the formation of two different counter-rotating vortices of which the centers are typically shifted to the corners of the cross-sections but located on opposite sides to each other. The square-wave channel shows a very complicated vortical structure, where more than four different counter-rotating vortices are visualized. Fig. 13 shows the velocity vector plots at a Reynolds number of 50 on four different planes that are indicated by AB, AC, AD, and EE, respectively, in the figure. At the plane AB that is just upstream of a turn, the flow patterns are almost the same for every channel, and there is no transverse flow. At the plane AC, two vortices are present in all the three channels. In the zig-zag channel, two vortices are located at the corner of the plane that are comparatively weaker than the vortices in the square-wave channel, and both square-wave and zig-zag channels commonly show the stronger velocity vectors at the middle of the plane, AC. On other hand, the curved channel shows the formation of two vortices with relatively uniform magnitudes of velocities over the whole of the plane AC. At the plane AD that is just downstream of the turn, the zig-zag and curved channels show the formation of two small vortices, while the square-wave channel shows the stronger vortices. At the plane EE, in the square-wave and curved channels, a pair of symmetric vortices with reduced strength is shown, while asymmetric vortices are shown in the zig-zag channel.

Fig. 14 shows the variation of the pressure drop for the three geometries at various Reynolds numbers. In all three cases, the pressure drops have been calculated for channels with equal streamwise lengths. The pressure drop is directly related to the energy input that is used for the mixing process. The pressure drops increase rapidly with the Reynolds number in all microchannels. When the Reynolds number is less than about 50, the pressure drops are almost the same in every channel. For Reynolds numbers that exceed 50, the pressure drops in the square-wave and the zig-zag channels are approximately the same, while the curved channel shows a considerably smaller pressure drop when compared to the other two channels because there is no sharp turn in the curved channel unlike the other channels.

4. Conclusion

In this work, a numerical study of mixing in different microchannels, i.e., zig-zag, square-wave, and curved channels, has been conducted. Water and ethanol have been selected as the two working fluids for mixing. Three-dimensional Navier–Stokes analyses for mixing and the flow field have been carried out for a wide range of the Reynolds number (Re = 0.267–267). In all the three microchannels, at low Reynolds numbers, i.e., at most about 5–15, depending on the type of the microchannel, the transverse flow is negligible, and thus, mixing occurs due to only the diffusion of fluid molecules, as a result of the higher residence time that obtains with a lower overall velocity. Therefore, the mixing is enhanced rapidly as the Reynolds number decreases in this range. In the range of Reynolds numbers, i.e., from 15 to 267, where the transverse motion of the flow prevails in the mixing process, the square-wave microchannel shows the best mixing performance, and the curved and zig-zag microchannels show nearly the same performance. However, at a Reynolds number of 267, the mixing index at the exit approaches the limiting value of about 0.9 in all the three cases. In all the microchannels, the pressure drops for channels with equal streamwise lengths rapidly increase with the Reynolds number. When the Reynolds number is at most about 50, the pressure drops are almost the same in every channel. For Reynolds numbers that exceed 50, the pressure drops in the square-wave and zig-zag channels are approximately the same, while the curved channel shows a considerably smaller pressure drop when compared to the other two channels because there is no sharp turn in the curved channel unlike the other channels.

Acknowledgement

This work was supported by INHA UNIVERSITY Research Grant.

References

[1] A. Maha, S.A. Soper, Simulation and design of micromixers for microfluidic devices, in microfluidics, in: BioMEMS and Medical Microsystems, SPIE, Bellingham, 2003.
[2] X.B. Wang, Y. Huang, J. Vykoukal, Cell separation by dielectrophoretic field flow fractionation, Anal. Chem. 72 (2000) 832–839.
[3] D. Gobby, P. Angeli, A. Gavriilidis, Mixing characteristics of T-type microfluidic mixers, J. Micromech. Microeng. 11 (2001) 126–132.
[4] M.A. Ansari, K.Y. Kim, Shape optimization of a micromixer with staggered herringbone groove, Chem. Eng. Sci. 62 (2007) 6687–6695.
[5] C.K. Chen, C.C. Cho, Electrokinetically driven flow mixing in microchannels with wavy surface, J. Colloid Interf. Sci. 312 (2007) 470–480.
[6] R.H. Liu, M.A. Stremler, K.V. Sharp, M.G. Olsen, J.G. Santiago, R.J. Adrian, H. Aref, D.J. Beebe, Passive mixing in a three-dimensional serpentine microchannel, J. Microelectromech. Syst. 9 (2) (2000) 190–197.
[7] M.A. Ansari, K.Y. Kim, Parametric study on mixing of two fluids in a three-dimensional serpentine microchannel, Chem. Eng. J. 146 (2009) 439–448.
[8] J.K. Chen, R.J. Yang, Electroosmotic flow mixing in zigzag microchannels, Electrophoresis 28 (6) (2007) 975–983.
[9] V. Mengeaud, J. Josserand, H.H. Girault, Mixing processes in a zigzag microchannel: finite element simulations and optical study, Anal. Chem. 74 (2002) 4279–4286.
[10] S.P. Vanka, G. Luo, C.M. Winkler, Numerical study of scalar mixing in curved channels at low Reynolds numbers, AICHE J. 50 (2004) 2359–2368.
[11] V. Khmar, M. Aggararwal, K.D.P. Nigam, Mixing in curve tubes, Chem. Eng. Sci. 61 (2006) 5742–5753.
[12] A.P. Sudarsan, V.M. Ugaz, Fluid mixing in planar spiral microchannels, Lab Chip 6 (2007) 74–82.
[13] S. Chang, Y.H. Cho, Static micromixers using alternating whirls and lamination, J. Micromech. Microeng. 15 (2005) 1397–1405.

[14] S.J. Park, J.K. Kim, J. Park, S. Chung, C. Chung, K. Chang, Rapid three-dimensional passive rotation micromixer using the breakup process, J. Micromech. Microeng. 12 (2004) 6–14.
[15] M.K. Jeon, J.H. Kim, J. Noh, S.H. Kim, H.G. Park, S.I. Woo, Design and characterization of a passive recycle micromixer, J. Micromech. Microeng. 15 (2005) 351–357.
[16] CFX-11.0, Solver Theory, ANSYS, 2007.
[17] S. Hardt, F. Schonfeld, Laminar mixing in different interdigital micromixers. II. Numerical simulations, AICHE J. 49 (3) (2003) 578–584.
[18] H. Wang 1, P. Iovenitti, E. Harvey, S. Masood, Optimizing layout of obstacles for enhanced mixing in microchannels, Smart Mater. Struct. 11 (2002) 662–667.
[19] J.T. Yang, K.W. Lin, Mixing and separation of two-fluid flow in a micro planner serpentain channel, J. Micromech. Microeng. 16 (2006) 2439–2448.